Structural and magnetic phase diagram of $CeFeAsO_{1-x}F_x$ and its relation to high-temperature superconductivity

JUN ZHAO[1], Q. HUANG[2], CLARINA DE LA CRUZ[1,3], SHILIANG LI[1], J. W. LYNN[2], Y. CHEN[2,4], M. A. GREEN[2,4], G. F. CHEN[5], G. LI[5], Z. LI[5], J. L. LUO[5], N. L. WANG[5] AND PENGCHENG DAI[1,3]*

[1]Department of Physics and Astronomy, The University of Tennessee, Knoxville, Tennessee 37996-1200, USA
[2]NIST Center for Neutron Research, National Institute of Standards and Technology, Gaithersburg, Maryland 20899-6012, USA
[3]Neutron Scattering Science Division, Oak Ridge National Laboratory, Oak Ridge, Tennessee 37831, USA
[4]Department of Materials Science and Engineering, University of Maryland, College Park, Maryland 20742-6393, USA
[5]Beijing National Laboratory for Condensed Matter Physics, Institute of Physics, Chinese Academy of Sciences, Beijing 100080, China
*e-mail: daip@ornl.gov

Published online: 26 October 2008; doi:10.1038/nmat2315

Recently, high-transition-temperature (high-T_c) superconductivity was discovered in the iron pnictide $RFeAsO_{1-x}F_x$ (R, rare-earth metal) family of materials. We use neutron scattering to study the structural and magnetic phase transitions in $CeFeAsO_{1-x}F_x$ as the system is tuned from a semimetal to a high-T_c superconductor through fluorine (F) doping, x. In the undoped state, CeFeAsO develops a structural lattice distortion followed by a collinear antiferromagnetic order with decreasing temperature. With increasing fluorine doping, the structural phase transition decreases gradually and vanishes within the superconductivity dome near $x = 0.10$, whereas the antiferromagnetic order is suppressed before the appearance of superconductivity for $x > 0.06$, resulting in an electronic phase diagram remarkably similar to that of the high-T_c copper oxides. Comparison of the structural evolution of $CeFeAsO_{1-x}F_x$ with other Fe-based superconductors suggests that the structural perfection of the Fe–As tetrahedron is important for the high-T_c superconductivity in these Fe pnictides.

A determination of the structural and magnetic phase transitions in doped transition-metal oxides is essential for understanding their electronic properties. For high-transition-temperature (high-T_c) copper oxides, the parent compounds are antiferromagnetic (AFM) Mott insulators[1]. When mobile 'electrons' or 'holes' are doped into the parent compounds, the static long-range AFM order is rapidly suppressed and optimal superconductivity emerges after a complete suppression of the static AFM order[2–5]. Much like in copper oxide superconductors, high-T_c superconductivity in the recently discovered rare-earth Fe-based oxide systems RFeAsO (R, rare-earth metal) and $(Ba_{1-x}K_x)Fe_2As_2$ is also derived from either electron[6–10] or hole[11,12] doping of their semimetal parent compounds. Although the parent compound LaFeAsO also exhibits long-range static AFM order that is suppressed on electron doping to induce superconductivity[13–15], there has been no systematic measurement to establish the doping evolution of the AFM order and its relationship to superconductivity. A determination of the structural, magnetic and superconductivity phase diagram in one of the RFeAsO systems will enable a direct comparison with the phase diagram of high-T_c copper oxides. Such a comparison is important because it might reveal whether the physics of high-T_c superconductivity in the Fe-based materials is fundamentally related to that of the high-T_c copper oxides[16–22].

Here, we report systematic neutron scattering studies of structural and magnetic phase transitions in the Fe pnictide $CeFeAsO_{1-x}F_x$ as the system is tuned from a semimetal to a high-T_c superconductor through F doping, x. We find that CeFeAsO undergoes a structural lattice distortion from tetragonal to orthorhombic structure near 155 K, followed by a commensurate AFM ordering on the Fe sublattice below ~140 K as shown in Figs 1 and 2, similar to that of LaFeAsO (ref. 13). Whereas the structural phase transition temperature decreases gradually with increasing F doping and disappears around $x = 0.1$ when superconductivity is already well developed (Fig. 3), the AFM ordering temperature and static Fe ordered moment reduce rapidly and essentially vanish before the emergence of superconductivity for $x > 0.06$. This results in the electron phase diagram shown in Fig. 1d, which is remarkably similar to that of the high-T_c copper oxides[2–5]. Therefore, although superconductivity in $CeFeAsO_{1-x}F_x$ can survive in either the low-temperature tetragonal or orthorhombic crystal structure, it competes directly with static AFM order.

Our detailed analysis of the low-temperature $CeFeAsO_{1-x}F_x$ structures reveals that F doping does not change the Fe–As distance but reduces the Ce–As distance and Fe–As–Fe angles (Fig. 4). These results suggest that the main effect of F doping is to transfer electrons from the Ce–O/F layers to the As–Fe–As block (Fig. 4a), thereby decreasing the distance between them with electron doping due to increased Coulomb attraction. Comparison of the structural evolution of $CeFeAsO_{1-x}F_x$ with other rare-earth Fe pnictides[10,13,23,24] and $(Ba_{1-x}K_x)Fe_2As_2$ (refs 12,25) suggests that the Fe–As–Fe bond angle decreases systematically for materials

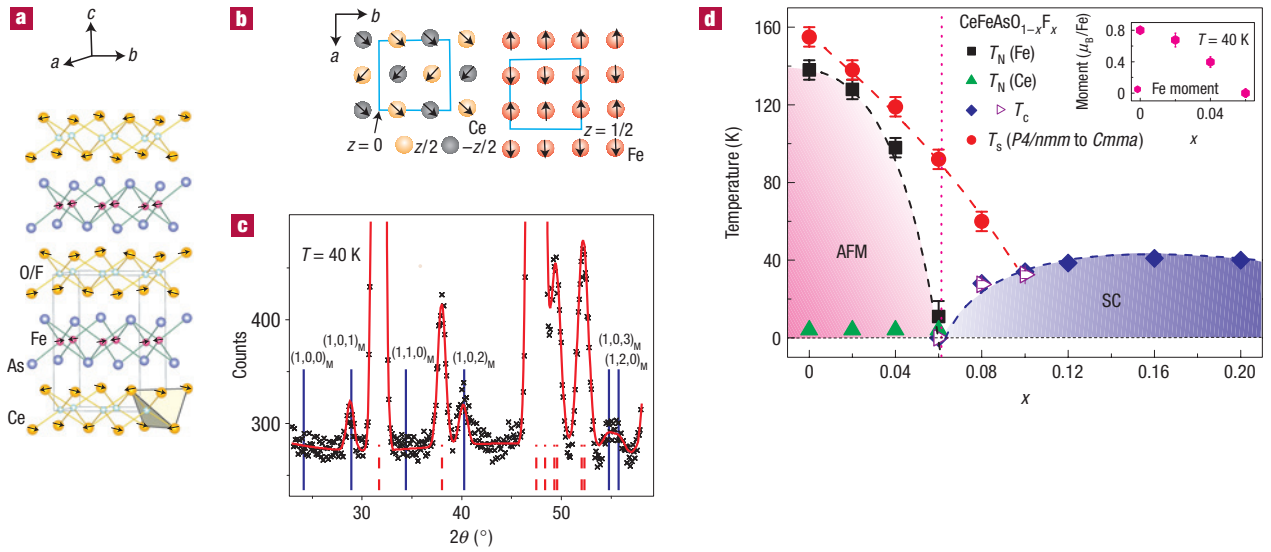

Figure 1 Low-temperature magnetic structures for Ce and Fe in CeFeAsO and the structural and magnetic phase diagram of $CeFeAsO_{1-x}F_x$. **a**, The three-dimensional antiferromagnetic structures of Ce and Fe as determined from our neutron diffraction data. **b**, The magnetic unit cells of Ce and Fe. The Fe moments lie in the *a*–*b* plane and form an antiferromagnetic collinear structure similar to that of LaFeAsO (ref. 13), whereas nearest-neighbour spins along the *c* axis are parallel and so there is no need to double the magnetic cell along the *c* axis. **c**, Observed (crosses) and calculated (solid line) neutron powder diffraction intensities of CeFeAsO at 40 K using space group *Cmma* for the nuclear structure and the structures in **a**,**b** for the magnetic structure. The dashed vertical lines indicate the expected nuclear Bragg peak positions and the solid vertical lines represent magnetic Bragg peak positions for the spin structure in the right panel of **b**. The data in **c** were collected using BT-7 with an incident beam wavelength $\lambda = 2.36$ Å with pyrolytic graphite (0,0,2) as a monochromator and a pyrolytic graphite filter. **d**, The structural and magnetic phase diagram determined from our neutron measurements on $CeFeAsO_{1-x}F_x$ with $x = 0$, 0.02, 0.04, 0.06, 0.08, 0.10, 0.16. The red circles indicate the onset temperature of the *P4/nmm* to *Cmma* phase transition. The black squares and green triangles designate the Néel temperatures of Fe, T_N(Fe), and Ce, T_N(Ce), respectively, as determined from neutron measurements in Fig. 2e–h. The superconducting transition temperatures for $x = 0.08$, 0.012, 0.016, 0.20 (blue diamond) are from the onset T_c of the resistivity measurements adapted from ref. 8. The open triangles are T_c determined from susceptibility measurements in Fig. 3. The inset in **d**, shows the F-doping dependence of the Fe moment as determined from the intensity of the $(1,0,2)_M$ magnetic peak at 40 K, where the influence of the Ce moment on the Fe magnetic Bragg peak intensity can be safely ignored. The error bars in **d** indicate one standard deviation.

with increasing T_c (Fig. 5). The results suggest that the structural perfection of the Fe–As tetrahedron is crucial for the high-T_c superconductivity in these Fe pnictides.

We use neutron diffraction to study the structural and magnetic phase transitions in polycrystalline non-superconducting $CeFeAsO_{1-x}F_x$ with $x = 0$, 0.02, 0.04 and 0.06 and superconducting $CeFeAsO_{1-x}F_x$ with $x = 0.08$, 0.10 and 0.16. T_c values for $x = 0.08$ and 0.10 are shown in the insets of Fig. 3a and b respectively, and T_c for $x = 0.16$ is 35 K; all measurements were determined by susceptibility measurements using a commercial superconducting quantum interference device. Our samples are made using the method described in ref. 8. Our neutron experiments were carried out on the BT-1 high-resolution powder diffractometer and BT-7 thermal triple-axis spectrometer at the NIST Center for Neutron Research, Gaithersburg, Maryland. Some measurements were also carried out on the HB-3 thermal triple-axis spectrometer at the High Flux Isotope Reactor, Oak Ridge National Laboratory.

In previous work, it was found that LaFeAsO undergoes a structural distortion below 155 K, changing the symmetry from tetragonal (space group *P4/nmm*) to monoclinic (space group $P112/n$) (ref. 13) or orthorhombic (space group *Cmma*) (ref. 26), followed by a long-range commensurate AFM order with a collinear spin structure below ~137 K (ref. 13). For convenience in comparing the low-temperature nuclear and magnetic structures, we use the orthorhombic *Cmma* space group to describe the low-temperature structural data in this article. As $CeFeAsO_{1-x}F_x$ has rare-earth Ce, which carries a local magnetic moment[8] and therefore is different from the non-magnetic La in $LaFeAsO_{1-x}F_x$ (ref. 13), we first need to determine whether this material has the same lattice distortion and magnetic structure as $LaFeAsO_{1-x}F_x$. Our high-resolution neutron powder diffraction measurements on BT-1 confirm that the lattice symmetry of CeFeAsO also exhibits the tetragonal to orthorhombic transition below ~158 K (Figs 1d and 2a), where the $(2,2,0)_T$ peak in the tetragonal phase is split into $(0,4,0)_O$ and $(4,0,0)_O$ peaks in the orthorhombic phase (Fig. 2a, inset).

To see if the Fe spins in CeFeAsO exhibit the same magnetic order as that of LaFeAsO (ref. 13), we carried out measurements on BT-7. The Ce moments order magnetically below ~4 K (ref. 8 and Fig. 2e), and thus we took data at 40 K to avoid any possible induced-moment influence of Ce on the intensities of the Fe magnetic peaks (Fig. 1c). Comparison of Fig. 1c with the same scan at 160 K (see Supplementary Information) and with Fig. 3c in ref. 13 for LaFeAsO immediately reveals that the Fe magnetic unit cell in CeFeAsO can be indexed as $\sqrt{2}a_N \times \sqrt{2}b_N \times c_N$, where a_N, b_N and c_N are nuclear lattice parameters of the unit cell (see Table 1). This indicates that CeFeAsO has the same collinear in-plane Fe AFM structure as that of LaFeAsO, but the *c*-axis nearest-neighbour spins are parallel in CeFeAsO rather than anti-parallel as in LaFeAsO. Hence, there is no need to double the unit cell along the *c* axis (Fig. 1a), and an excellent fit to the data is achieved using the magnetic and nuclear unit cells in Fig. 1a,b, as shown by the solid red line in Fig. 1c. The ordered iron moment is $0.8(1)\,\mu_B$ at 40 K, where numbers in parentheses indicate uncertainty in the last decimal place and μ_B denotes the Bohr magneton. The magnitude of the Fe moment

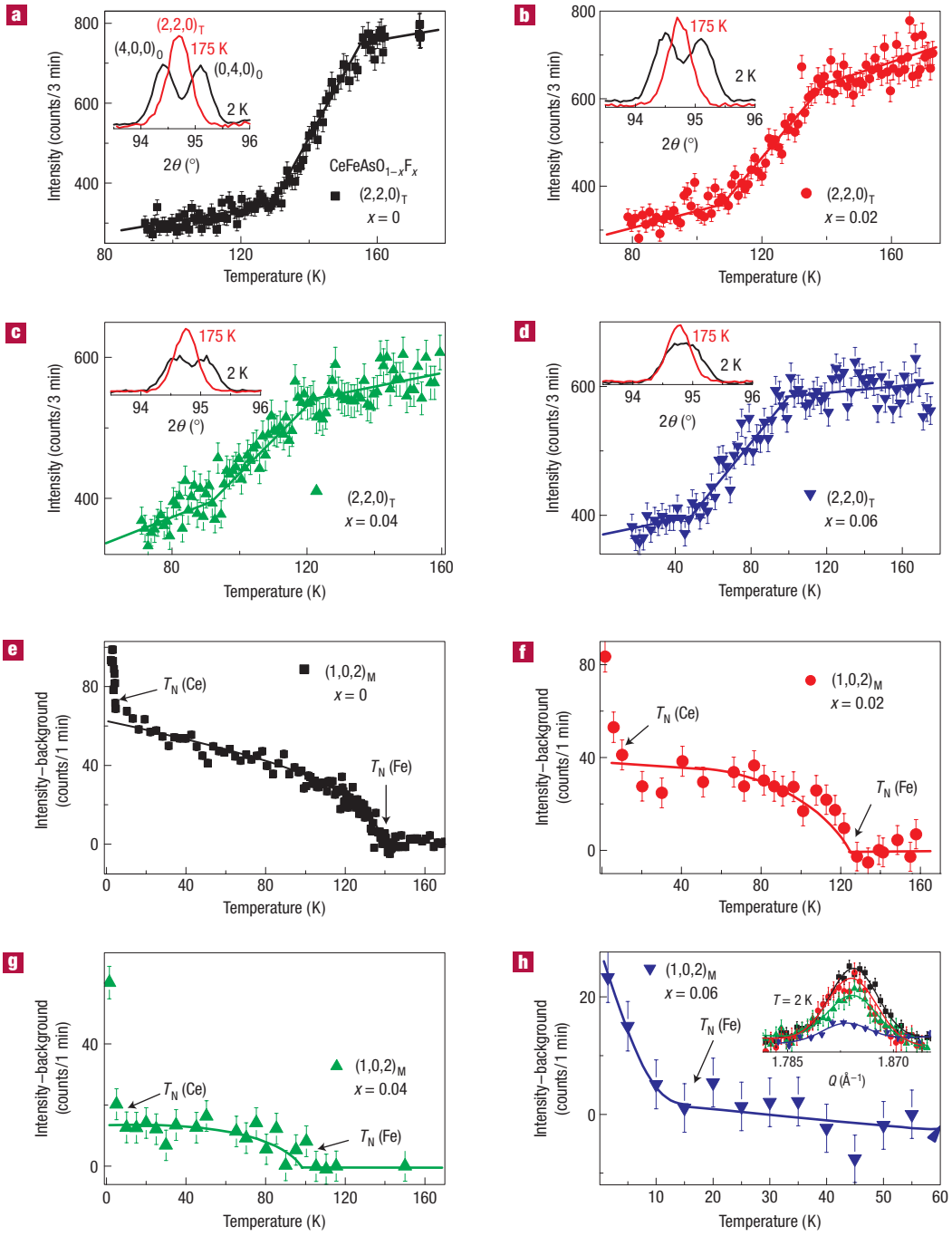

Figure 2 Structural and magnetic phase transition temperatures as a function of increasing F doping in $CeFeAsO_{1-x}F_x$. The data in **a–d** and **e–g** were collected on BT-1 and BT-7, respectively. The ***Q***-scans for $x = 0.06$ (inset in **h**) were carried out on HB-3 using a similar set-up as BT-7. The BT-1 diffractometer has a Ge(3,1,1) monochromator and an incident beam wavelength of $\lambda = 2.0785$ Å. **a–d**, Temperature dependence of the $(2,2,0)_T$ (T denotes tetragonal) neutron scattering nuclear reflection intensity (vertical axes) indicative of a structural phase transition[13] for various x. The insets show the neutron scattering $(2,2,0)_T$ reflection intensity (in arbitrary units) as a function of scattering angle above and below the transition temperatures[13]. **e–h**, Temperature dependence of the order parameter at the magnetic Bragg peak position $(1,0,2)_M$ as a function of F doping. The intensity in vertical axes is obtained by subtracted the measured $(1,0,2)_M$ peak intensity from the background scattering at positions away from the Bragg peak. The large increase in intensity below 4 K is due to Ce ordering, as confirmed by the temperature dependence of the Ce-only magnetic Bragg peak $(0,0,1)_M$ (see Supplementary Information). The inset in **h** shows the doping dependence of the $(1,0,2)_M$ Bragg peak normalized to the nuclear Bragg peak intensity. The peak positions and widths are essentially doping independent, suggesting that the AFM order is commensurate at all doping levels. The error bars indicate one standard deviation.

in CeFeAsO is about twice that of the Fe ordered moment in LaFeAsO (ref. 13). We also determined the Ce magnetic structure using data collected at 1.7 K (see Supplementary Information) and found a strong coupling between the Fe and Ce moments below 20 K (Fig. 2e–g). The Ce and Fe ordered moments at 1.7 K are $0.83(2)\ \mu_B$/Ce and $0.94(3)\ \mu_B$/Fe, respectively. Our determined

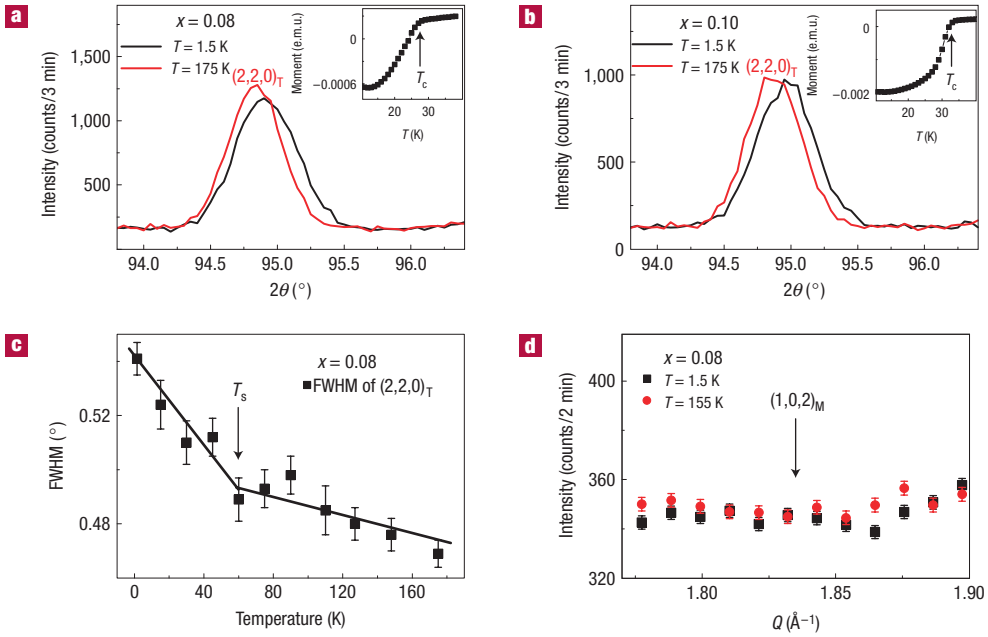

Figure 3 Low-temperature lattice structure and tetragonal to orthorhombic structural phase transition temperature for superconducting $CeFeAsO_{1-x}F_x$ with $x = 0.08$ and 0.10. The data were collected on BT-1 and BT-7 using an identical experimental set-up to that of Fig. 2. **a**,**b**, Comparison of the $(2,2,0)_T$ (T denotes tetragonal) nuclear reflection at 175 K and 1.5 K for $x = 0.08$ and 0.10. In both cases, the width at 1.5 K is broader than that at 175 K. However, the width is larger in the case of $x = 0.08$ at 1.5 K. The insets show the superconductivity transition temperature of the neutron samples measured by a superconducting quantum interference device. **c**, Temperature dependence of the $(2,2,0)_T$ Bragg peak width for the $x = 0.08$ sample, which shows a clear kink around 60 K, indicating a tetragonal to orthorhombic phase transition. **d**, Comparison of the scattering near the $(1,0,2)_M$ position (as marked by the arrow) for the $x = 0.08$ sample at 1.5 K and 155 K. The data are featureless, indicating no static long-range AFM order. The error bars indicate one standard deviation.

Ce and Fe magnetic structures are shown in Fig. 1a,b. However, we caution the reader that future single-crystal work might be necessary to confirm the proposed Ce spin structure in Fig. 1a. The lack of the *c*-axis unit-cell doubling in the Fe magnetic structure of CeFeAsO is different from that of LaFeAsO, but identical to the Fe spin structure in PrFeAsO, which has an Fe ordered moment of 0.48(9) μ_B/Fe (refs 27,28). On the other hand, Fe magnetic ordering in NdFeAsO has the same spin structure as LaFeAsO but with a moment of only 0.25(7) μ_B/Fe (ref. 29). Assuming that the observed AFM order in different rare-earth oxypnictides indeed arises from a spin-density-wave (SDW) instability in a nested Fermi surface[19–21,30], it is unclear how the different observed Fe AFM structures/moments for different rare-earth oxypnictides can be explained by their differences in band structures, as most of the calculations are carried out for LaFeAsO.

Having shown that the lattice distortion and Fe magnetic unit cells are similar between CeFeAsO and LaFeAsO, it is important to determine the evolution of the lattice and magnetic structures with increasing F doping as superconductivity is induced. If the collinear AFM order in CeFeAsO and LaFeAsO is a SDW instability arising from a nested Fermi surface[19–21,30] similar to that of the pure metallic Cr (refs 31,32), electron doping will change the electron and hole pocket sizes, but may induce incommensurate SDW order[33]. For Cr (refs 31,32), where the SDW order has a long-wavelength incommensurate magnetic structure, electron/hole doping quickly locks the SDW to commensurate antiferromagnetism with an ordered moment that is doping independent[31]. Figure 2 summarizes the structural and magnetic phase transition data for $CeFeAsO_{1-x}F_x$ with $x = 0$, 0.02, 0.04 and 0.06. Inspection of Fig. 2a–d and its insets immediately reveals that the onset lattice distortion temperature (seen as the initial drop in the $(2,2,0)_T$ peak intensity) and the magnitude of the lattice distortion (the low-temperature splitting of the $(0,4,0)_O$ and $(4,0,0)_O$ peaks) both decrease gradually with increasing x (Fig. 1d). On the other hand, the wave-vector positions and coherence-length limits of the $(1,0,2)_M$ magnetic peaks ($\boldsymbol{Q} = 1.838(1)$, 1.833(1), 1.837(1) and 1.831(3) Å^{-1}; and $\xi = 140(6)$, 137(8), 134(11) and 140(30) Å for $x = 0$, 0.02, 0.04 and 0.06, respectively (Fig. 2g, inset)) are doping independent, and indicate no observable commensurate to incommensurate phase transition. The integrated intensity of the $(1,0,2)_M$ magnetic peak decreases rapidly with increasing x and essentially vanishes near $x = 0.06$ (Fig. 1d, inset). The corresponding Néel temperatures for T_N(Fe) and T_N(Ce) are determined by measuring the temperature dependence of the $(1,0,2)_M$ magnetic reflection (Fig. 2e–h).

To see if the tetragonal to orthorhombic structural phase transition in $CeFeAsO_{1-x}F_x$ can survive superconductivity, which appears for samples with $x > 0.06$ (ref. 8), we carried out extra measurements on $x = 0.08$ and 0.10 samples at BT-1 and BT-7. Susceptibility measurement data in the insets of Fig. 3a,b show the onset of superconductivity at 27 K and 33 K for $x = 0.08$ and 0.10 samples, respectively. Although the $(2,2,0)_T$ peak does not reveal a clear splitting at 1.5 K indicative of an orthorhombic distortion for the $x = 0.08$ sample, its width at low temperature is clearly broader than that at 175 K owing to the orthorhombic distortion (Fig. 3a). Detailed analysis of the BT-1 spectra confirms that the *Cmma* space group describes the low-temperature data better than the *P4/nmm* space group, thus indicating that superconductivity can survive in either the tetragonal or orthorhombic crystal structure. To determine the tetragonal to orthorhombic phase transition temperature, we carefully measured the temperature-dependent profile of the

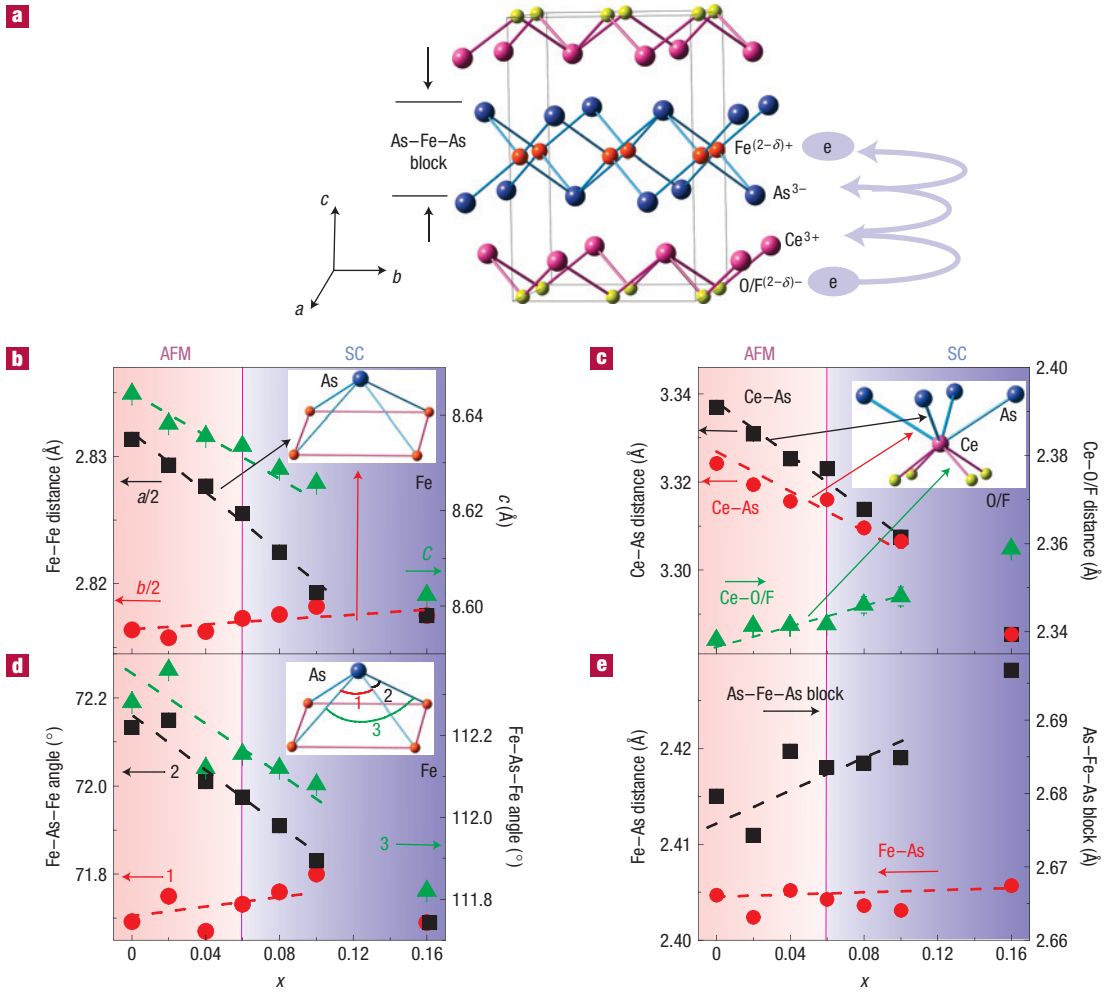

Figure 4 Low-temperature structural evolution of $CeFeAsO_{1-x}F_x$ as a function of F doping obtained from analysis of the BT-1 data. The atomic positions of $CeFeAsO_{1-x}F_x$ are shown in Table 2 and the effect of F doping is to expand the Fe–As–Fe block and to move the Ce–O/F block closer to the Fe–As–Fe block, thereby facilitating electron doping to the superconducting Fe–As–Fe layer. **a**, Schematic diagram defining the Fe–As–Fe block and illustrating the process of electron doping. **b**, *a*, *b* and *c* lattice constants of the orthorhombic unit cell and the two Fe–Fe nearest-neighbour distances as a function of F doping. There is no observable anomaly across the antiferromagnetic to superconductivity phase boundary around $x = 0.06$. **c**, Ce–O/F and Ce–As distances as a function of F doping. The slight increase in the Ce–O/F block size is compensated by much larger reduction in the Ce–As distance, resulting in an overall *c*-axis lattice contraction as shown in **b**. **d**, Fe–As–Fe bond angles as defined in the inset versus F doping. Whereas angle 1 hardly changes with doping, angles 2 and 3 decrease substantially with increasing F doping. **e**, The Fe–As bond distance and As–Fe–As block size versus F doping. The Fe–As distance is independent of F doping. The error bars indicate one standard deviation.

$(2,2,0)_T$ peak. Figure 3c shows the full-width at half-maximum (FWHM) of the peak as a function of temperature and it is clear that the tetragonal to orthorhombic phase transition occurs near 60 K. For comparison, we also carried out similar measurements for the $x = 0.10$ sample (Fig. 3b). Although analysis of the low-temperature BT-1 spectrum again suggests that the *Cmma* space group fits the data better than the *P4/nmm* space group, the diminishing differences between the tetragonal and orthorhombic crystal structures means we were unable to determine a structural phase transition temperature. Thermal triple-axis measurements on the $x = 0.08$ sample reveal no evidence of static long-range AFM Fe ordering (Fig. 3d), thus suggesting that static AFM order competes directly with superconductivity. To summarize the systematic work of Figs 2 and 3, we plot in Fig. 1d the structural and magnetic phase diagram of $CeFeAsO_{1-x}F_x$ together with superconducting transition temperatures determined from susceptibility measurements on neutron samples and earlier work[8]. These results are remarkably similar to the phase diagram of copper oxides[2–5], and may have important theoretical implications[16–18].

Figure 4 summarizes the impact of F doping on the crystal structure of $CeFeAsO_{1-x}F_x$ obtained from our detailed refinement analysis of the BT-1 data. The undoped CeFeAsO has an orthorhombic low-temperature structure with $c > a > b$ (Fig. 4a). Doping fluorine gradually suppresses both the *a*- (the long Fe–Fe nearest-neighbour distance) and *c*-axis lattice constants while leaving the *b* axis (the short Fe–Fe nearest-neighbour distance) essentially unchanged (Fig. 4b). The system almost becomes tetragonal at $x = 0.10$ with $a = b$, and the *c*-axis lattice constant continues to decrease with increasing doping for $x > 0.10$. The reduction in the *c*-axis lattice constant is achieved through a large reduction of the Ce–As distance, while the Ce–O/F and As–Fe–As block distances actually increase with increasing F doping (Fig. 4c,e). This suggests that the effect of F doping is to bring

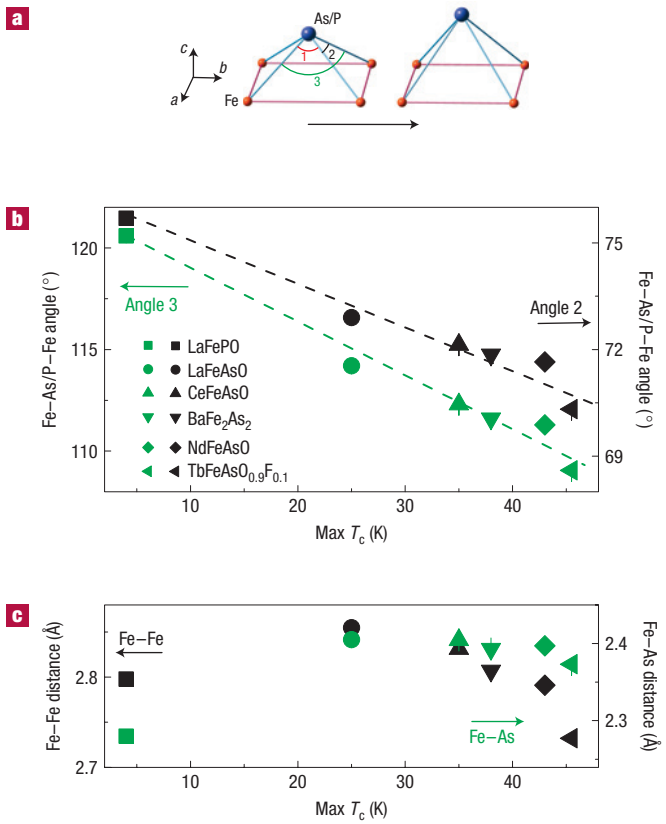

Figure 5 Fe–As(P)–Fe bond angles, Fe–Fe and Fe–As(P) distances for different Fe-based superconductors. There is a systematic decrease in the Fe–As(P)–Fe bond angle for Fe-based superconductors with higher T_c, suggesting that the lattice effects are important. **a**, Schematic diagram of what happens to the Fe–As–Fe tetrahedron for Fe-based superconductors as a function of increasing T_c. **b**,**c**, Dependence of the maximum T_c on Fe–As(P)–Fe angle (**b**) and Fe–Fe/Fe–As(P) distance (**c**). The Fe–As(P)–Fe angles and Fe–Fe/Fe–As(P) distances are computed using atomic positions given in refs 24,37 for LaFePO, ref. 13 for LaFeAsO, present paper for CeFeAsO, ref. 25 for $BaFe_2As_2$, ref. 38 for NdFeAsO and ref. 10 for $TbFeAsO_{0.9}F_{0.1}$. The maximum T_c is obtained when the Fe–As(P)–Fe bond angle reaches the ideal value of 109.47° for the perfect FeAs tetrahedron. Note here we used the maximum T_c obtained from susceptibility measurements, which is lower than that of the resistivity measurement on the same system. The error bars indicate one standard deviation.

the Ce–O/F charge transfer layer closer to the superconducting As–Fe–As block, thereby facilitating electron charge transfer (Fig. 4a) as confirmed by recent X-ray absorption spectroscopy measurements[34]. As the Fe–As distance (2.405 Å) is essentially doping independent (Fig. 4e), the strong hybridization between the Fe 3*d* and the As 4*p* orbitals[35] is not affected by electron doping. On the other hand, if we assume that the Fe–Fe nearest-neighbour (J_1) and next-nearest-neighbour effective exchange couplings (J_2) are mediated through the electron Fe–As–Fe hopping and controlled by the Fe–As–Fe angles[36], Fig. 4d suggests that J_2 and one of the nearest-neighbour exchange constants (J_1) decrease with increasing F doping while the other J_1 remains unchanged.

In a previous study on the phase diagram of oxygen-deficient $RFeAsO_{1-\delta}$ (ref. 9), it was found that systematically replacing *R* from La to Ce, Pr, Nd and Sm in $RFeAsO_{1-\delta}$ resulted in a gradual decrease in the *a*-axis lattice parameters and an increase in T_c. If T_c for different Fe-based superconductors is indeed correlated to their structural properties, a systematic trend between T_c and the Fe–As–Fe bond angles would be expected to be found, because the exchange couplings (J_1 and J_2) are directly related to the Fe–As–Fe bond angles[16,36] (Fig. 5a). Figure 5b,c shows the Fe–As(P)–Fe angles and Fe–Fe/Fe–As(P) distances versus maximum T_c for different Fe-based rare-earth oxypnictides[13,23–26,37,38] and $Ba_{1-x}K_xFe_2As_2$ (ref. 12) superconductors. Although the Fe–Fe/Fe–As(P) distances may not have a clear trend amongst different Fe-based superconductors (Fig. 5c), it is remarkable that the maximum T_c seems to be directly related to the Fe–As(P)–Fe angles for a variety of materials (Fig. 5b) and the highest T_c is obtained when the Fe–As(P)–Fe angle reaches the ideal value of 109.47° for the perfect FeAs tetrahedron with the least lattice distortion. This suggests that the most effective way to increase T_c in Fe-based superconductors is to decrease the deviation of the Fe–As(P)–Fe bond angle from the ideal FeAs tetrahedron, as the geometry of the FeAs tetrahedron might be correlated with the density of states near the Fermi energy.

In summary, we have mapped out the structural and magnetic phase transitions of $CeFeAsO_{1-x}F_x$ and found that the Fe static AFM order essentially vanishes before the appearance of superconductivity[39]. The phase diagram of $CeFeAsO_{1-x}F_x$ is therefore remarkably similar to that of the electron-doped high-T_c copper oxides[4,5]. In a recent μSR and ^{57}Fe Mössbauer spectroscopy study on the phase diagram of $LaFeAsO_{1-x}F_x$, Luetkens *et al.*[40] argue that the antiferromagnetism to superconductivity transition is first order and the orthorhombic structure does not coexist with superconductivity. In contrast, X-ray scattering[41] and μSR experiments[42] on $SmFeAsO_{1-x}F_x$ suggest coexistence of static antiferromagnetism and the orthorhombic structure with superconductivity in the underdoped regime. Although our neutron diffraction experiments confirm no static AFM order for $LaFeAsO_{1-x}F_x$ at $x = 0.05$, consistent with the μSR study[40], we find clear evidence for the orthorhombic lattice distortion[43]. These results suggest that the orthorhombic structure can survive superconductivity in $LaFeAsO_{1-x}F_x$, much like $CeFeAsO_{1-x}F_x$ discussed here and $SmFeAsO_{1-x}F_x$ (ref. 41). As superconductivity in the $LaFeAsO_{1-x}F_x$ (refs 6,40), $CeFeAsO_{1-x}F_x$

Table 1 Refined structure parameters of $CeFeAsO_{1-x}F_x$ with $x = 0$ at 175 K and $x = 0.16$ at 60 K. Space group: *P4/nmm*. CeFeAsO, $a = 3.99591(5)$, $c = 8.6522(1)$ Å; $CeFeAsO_{0.84}F_{0.16}$, $a = 3.98470(3)$, $c = 8.6032(1)$ Å.

Atom	Site	*x*	*y*	*z* (*x* = 0)	*B* (Å^2) (*x* = 0)	*z* (*x* = 0.16)	*B* (Å^2) (*x* = 0.16)
Ce	2*c*	1/4	1/4	0.1413(3)	0.34(4)	0.1480(4)	0.58(5)
Fe	2*b*	3/4	1/4	1/2	0.25(4)	1/2	0.09(3)
As	2*c*	1/4	1/4	0.6546(2)	0.28(3)	0.6565(3)	0.27(4)
O	2*a*	3/4	1/4	0	0.30(5)	0	0.50(4)

$x = 0$, $Rp = 5.02\%$, $wRp = 6.43\%$, $\chi^2 = 1.336$;
$x = 0.16$, $Rp = 5.94\%$, $wRp = 8.24\%$, $\chi^2 = 2.525$.
Here χ^2 is goodness of fit and *Rp* and *wRp* are residuals of observed and calculated intensities.

Table 2 Refined structure parameters of $CeFeAsO_{1-x}F_x$ with $x = 0$, 0.02, 0.04, 0.06, 0.08, 0.10 at 1.4 K. Space group: *Cmma*. Atomic positions: Ce: 4*g* (0, 1/4, *z*); Fe: 4*b* (1/4, 0, 1/2), As: 4*g* (0, 1/4, *z*) and O/F: 4*a* (1/4, 0, 0).

Atom		$x = 0$	$x = 0.02$	$x = 0.04$	$x = 0.06$	$x = 0.08$	$x = 0.10$
	a (Å)	5.66263(4)	5.65865(9)	5.6553(1)	5.6511(1)	5.6450(2)	5.6386(7)
	b (Å)	5.63273(4)	5.63155(9)	5.6325(1)	5.6346(1)	5.6352(2)	5.6364(7)
	c (Å)	8.64446(7)	8.6382(1)	8.6355(2)	8.6335(1)	8.6287(1)	8.6258(2)
Ce	*z*	0.1402(2)	0.1417(4)	0.1419(4)	0.1420(3)	0.1432(4)	0.1439(5)
	B (Å^2)	0.36(2)	0.37(6)	0.31(6)	0.46(5)	0.18(6)	0.51(6)
Fe	*B* (Å^2)	0.34(2)	0.38(4)	0.30(3)	0.34(3)	0.06(3)	0.14(4)
As	*z*	0.6553(1)	0.6548(3)	0.6555(3)	0.6554(2)	0.6555(3)	0.6556(3)
	B (Å^2)	0.45(2)	0.50(6)	0.36(5)	0.24(4)	0.17(5)	0.18(5)
O/F	*B* (Å^2)	0.54(2)	0.53(6)	0.64(6)	0.63(5)	0.24(5)	0.44(6)
	Rp (%)	4.31	5.44	4.90	4.71	4.66	5.01
	wRp (%)	5.60	6.72	6.31	6.16	5.92	6.34
	χ^2	2.192	1.258	0.966	0.9622	1.067	1.023

(ref. 8) and $SmFeAsO_{1-x}F_x$ (refs 41,42,44) systems first appears for $x = 0.05$, 0.08 and 0.10, respectively, it is possible that the first-order-like phase transition between antiferromagnetism and superconductivity in $LaFeAsO_{1-x}F_x$ (ref. 40) gradually evolves into that shown in Fig. 1d for $CeFeAsO_{1-x}F_x$ before becoming that for $SmFeAsO_{1-x}F_x$ (refs 41,42,44).

In addition to suppressing the static antiferromagnetism and inducing superconductivity, F doping also reduces the long axis of the orthorhombic structure and decreases the Fe–As–Fe bond angles. Comparison of the structural parameters of various Fe-based superconductors reveals that the Fe–As(P)–Fe bond angle decreases systematically for superconductors with increasing T_c values and reaches its maximum value for the ideal FeAs tetrahedral angle. This means that the structural distortion from the ideal FeAs tetrahedron is critical to the superconducting transition temperature and must be taken into account as we consider a mechanism for high-T_c superconductivity in these Fe-based materials.

Received 3 July 2008; accepted 26 September 2008; published 26 October 2008.

References

1. Lee, P. A., Nagaosa, N. & Wen, X.-G. Doping a Mott insulator: Physics of high-temperature superconductivity. *Rev. Mod. Phys.* **78**, 17–85 (2006).
2. Birgeneau, R. J., Stock, C., Tranquada, J. M. & Yamada, K. Magnetic neutron scattering in hole-doped cuprate superconductors. *J. Phys. Soc. Jpn* **75**, 111003 (2006).
3. Tranquada, J. M. in *Handbook of High-Temperature Superconductivity* (eds Schrieffer, J. R. & Brooks, J. S.) 257 (Springer, 2007).
4. Fujita, M. *et al.* Magnetic and superconducting phase diagram of electron-doped $Pr_{1-x}LaCe_xCuO_4$. *Phys. Rev. B* **67**, 014514 (2003).
5. Yu, W., Higgins, J. S., Bach, P. & Greene, R. L. Transport evidence of a magnetic quantum phase transition in electron-doped high-temperature superconductors. *Phys. Rev. B* **76**, 020503(R) (2007).
6. Kamihara, Y., Watanabe, T, Hirano, M. & Hosono, H. Iron-based layered superconductor $LaO_{1-x}F_xFeAs$ ($x = 0.05$–0.12) with $T_c = 26$ K. *J. Am. Chem. Soc.* **130**, 3296–3297 (2008).
7. Chen, X. H. *et al.* Superconductivity at 43 K in $SmFeAsO_{1-x}F_x$. *Nature* **453**, 761–762 (2008).
8. Chen, G. F. *et al.* Superconductivity at 41 K and its competition with spin-density-wave instability in layered $CeO_{1-x}F_xFeAs$. *Phys. Rev. Lett.* **100**, 247002 (2008).
9. Ren, Z.-A. *et al.* Superconductivity and phase diagram in the iron-based arsenic-oxides $ReFeAsO_{1-\delta}$ (Re = rare earth metal) without F-Doping. *Euro. Phys. Lett.* **83**, 17002 (2008).
10. Bos, J.-W. G. *et al.* High pressure synthesis of late rare earth RFeAs(O,F) superconductors: R = Tb and Dy. *Chem. Commun.* 3634–3635 (2008).
11. Wen, H. H., Mu, G., Fang, L., Yang, H. & Zhu, X. Y. Superconductivity at 25 K in hole-doped $La_{1-x}Sr_xOFeAs$. *Euro. Phys. Lett.* **82**, 17009 (2008).
12. Rotter, M., Tegel, M. & Johrendt, D. Superconductivity at 38 K in the iron arsenide $Ba_{1-x}K_xFe_2As_2$. *Phys. Rev. Lett.* **101**, 107006 (2008).
13. de la Cruz, C. *et al.* Magnetic order close to superconductivity in the iron-based layered $LaO_{1-x}F_xFeAs$ systems. *Nature* **453**, 899–902 (2008).
14. Kitao, S. *et al.* Spin ordering in LaOFeAs and its suppression in superconductor $LaO_{0.89}F_{0.11}FeAs$ probed by Mössbauer spectroscopy. *J. Phys. Soc. Jpn* **77**, 103706 (2008).
15. Carlo, J. P. *et al.* μSR studies of RE(O,F)FeAs (RE = La, Nd, Ce) and LaOFeP systems: Possible incommensurate/stripe magnetism and superfluid density. Preprint at <http://arxiv.org/abs/0805.2186v1> (2008).
16. Si, Q. & Abrahams, E. Strong correlations and magnetic frustration in the high T_c iron pnictides. *Phys. Rev. Lett.* **101**, 076401 (2008).
17. Fang, C., Yao, H., Tsai, W. F., Hu, J. P. & Kivelson, S. A. Theory of electron nematic order in LaOFeAs. *Phys. Rev. B* **77**, 224509 (2008).
18. Xu, C. K., Müller, M. & Sachdev, S. Ising and spin orders in iron-based superconductors. *Phys. Rev. B* **78**, 020501(R) (2008).
19. Mazin, I. I., Singh, D. J., Johannes, M. D. & Du, M. H. Unconventional superconductivity with a sign reversal in the order parameter of $LaFeAsO_{1-x}F_x$. *Phys. Rev. Lett.* **101**, 057003 (2008).
20. Yin, Z. P. *et al.* Electron–hole symmetry and magnetic coupling in antiferromagnetic LaFeAsO. *Phys. Rev. Lett.* **101**, 057001 (2008).
21. Ma, F. J. & Lu, Z.-Y. Iron-based layered compound LaFeAsO is an antiferromagnetic semimetal. *Phys. Rev. B* **78**, 033111 (2008).
22. Haule, K. & Kotliar, G. Coherence-incoherence crossover in the normal state of iron-oxypnictides and importance of the Hund's rule coupling. Preprint at <http://arxiv.org/abs/0805.0722v1> (2008).
23. Tegel, M., Schellenberg, I., Röttgen, R. & Johrendt, D. A ^{57}Fe Mössbauer spectroscopy study of the 7 K superconductor LaFePO. Preprint at <http://arxiv.org/abs/0805.1208> (2008).
24. McQueen, T. M. *et al.* Intrinsic properties of stoichiometric LaOFeP. *Phys. Rev. B* **78**, 024521 (2008).
25. Rotter, M. *et al.* Spin density wave anomaly at 140 K in the ternary iron arsenide $BaFe_2As_2$. *Phys. Rev. B* **78**, 020503(R) (2008).
26. Nomura, T. *et al.* Crystallographic phase transition and high-T_c superconductivity in LaOFeAs:F. Preprint at <http://arxiv.org/abs/0804.3569> (2008).
27. Kimber, S. A. J. *et al.* Magnetic ordering and negative thermal expansion in PrFeAsO. *Phys. Rev. B* **78**, 140503 (2008).
28. Zhao, J. *et al.* Lattice and magnetic structures of PrFeAsO, $PrFeAsO_{0.85}F_{0.15}$, and $PrFeAsO_{0.85}$. *Phys. Rev. B* **78**, 132504 (2008).
29. Chen, Y. *et al.* Magnetic order of the iron spins in NdOFeAs. *Phys. Rev. B* **78**, 064515 (2008).
30. Dong, J. *et al.* Competing orders and spin-density-wave instability in $LaO_{1-x}F_xFeAs$. *Euro. Phys. Lett.* **83**, 27006 (2008).
31. Komura, S., Hamaguchi, Y. & Kunitomi, N. Experimental test of rigid band models for Cr by means of Cr–V–Mn ternary dilute alloys. *J. Phys. Soc. Jpn* **23**, 171–179 (1967).
32. Facett, E. Spin-density-wave antiferromagnetism in chromium. *Rev. Mod. Phys.* **60**, 209–283 (1988).
33. Maier, T. A. & Scalapino, D. J. Neutron scattering as a probe of the Fe-pnicitide superconducting gap. *Phys. Rev. B* **78**, 020514 (2008).
34. Zhang, C. L. *et al.* X-ray absorption spectroscopy measurement on the $LaO_{1-x}Fe_xFeAs$ system. Preprint at <http://arxiv.org/abs/0808.2134> (2008).
35. Wu, J. S., Phillips, P. & Castro Neto, A. H. Theory of the magnetic moment in iron pnictides. *Phys. Rev. Lett.* **101**, 126401 (2008).
36. Yildirim, T. Origin of the ~150 K anomaly in LaOFeAs; competing antiferromagnetic superexchange interactions, frustration, and structural phase transition. *Phys. Rev. Lett.* **101**, 057010 (2008).
37. Kamihara, Y. *et al.* Iron-based layered superconductor: LaOFeP. *J. Am. Chem. Soc.* **128**, 10012–10013 (2006).
38. Qiu, Y. *et al.* Structure and magnetic order in the $NdFeAsO_{1-x}F_x$ superconductor system. Preprint at <http://arxiv.org/abs/0806.2195v4> (2008).
39. Tarantini, C *et al.* Can antiferromagnetism and superconductivity coexist in the high-field paramagnetic superconductor Nd(O,F)FeAs? Preprint at <http://arxiv.org/abs/0805.4445v1> (2008).
40. Luetkens, H. *et al.* Electronic phase diagram of the $LaO_{1-x}F_xFeAs$ superconductor. Preprint at <http://arxiv.org/abs/0806.3533> (2008).
41. Margadonna, S. *et al.* Crystal structure and phase transitions across the metal-superconductor boundary in the $SmFeAsO_{1-x}F_x$ ($0 < x < 0.20$) family. Preprint at <http://arxiv.org/abs/0806.3962> (2008).
42. Drew, A. J. *et al.* Coexistence of static magnetism and superconductivity in $SmFeAsO_{1-x}F_x$ as revealed by muon spin rotation. Preprint at <http://arxiv.org/abs/0807.4876> (2008).
43. Huang, Q. *et al.* Doping evolution of antiferromagnetic order and structure distortion in $LaFeAsO_{1-x}F_x$. *Phys. Rev. B* **78**, 054529 (2008).
44. Liu, R. H. *et al.* Anomalous transport properties and phase diagram of the FeAs based $SmFeAsO_{1-x}F_x$ superconductors. *Phys. Rev. Lett.* **101**, 087001 (2008).

Supplementary Information accompanies the paper at www.nature.com/naturematerials.

Acknowledgements

We thank E. Dagotto, A. Moreo, R. Fishman and T. Maier for helpful discussions. We also thank J. L. Zarestky for his help on the HB-3 measurements. This work is supported by the US National Science Foundation through DMR-0756568 and by the US Department of Energy, Division of Materials Science, Basic Energy Sciences, through DOE DE-FG02-05ER46202. This work is also supported in part by the US Department of Energy, Division of Scientific User Facilities, Basic Energy Sciences. The work at the Institute of Physics, Chinese Academy of Sciences, is supported by the National Science Foundation of China, the Chinese Academy of Sciences ITSNEM and the Ministry of Science and Technology of China.

Author information

Reprints and permissions information is available online at http://npg.nature.com/reprintsandpermissions. Correspondence and requests for materials should be addressed to P.D.